



Cite this: *Green Chem.*, 2023, 25, 1326

Received 19th November 2022,  
Accepted 26th January 2023

DOI: 10.1039/d2gc04368h

rsc.li/greenchem

## Identifying the optimal oxidation state of Cu for electrocatalytic reduction of CO<sub>2</sub> to C<sub>2+</sub> products†

Liang Xu,<sup>a</sup> Jiaqi Feng,<sup>a</sup> Limin Wu,<sup>a,b</sup> Xinning Song,<sup>a,b</sup> Xingxing Tan,<sup>a,b</sup> Libing Zhang,<sup>a,b</sup> Xiaodong Ma,<sup>a,b</sup> Shunhan Jia,<sup>a,b</sup> Juan Du,<sup>c</sup> Aibing Chen,<sup>c</sup> Xiaofu Sun<sup>\*,a,b</sup> and Buxing Han<sup>\*,a,b,d</sup>

The electrocatalytic CO<sub>2</sub> reduction reaction (CO<sub>2</sub>RR) to C<sub>2+</sub> products is of great importance. It is known that the co-operation of Cu<sup>1+</sup> and Cu<sup>0</sup> in the catalysts can yield a high faradaic efficiency (FE). However, it is very difficult to figure out the optimal ratio of Cu<sup>1+</sup> and Cu<sup>0</sup> because Cu<sup>1+</sup> can be reduced to Cu<sup>0</sup> during CO<sub>2</sub>RR. To solve this problem and identify the optimal oxidation state of Cu, herein we propose a strategy to prepare Cu catalysts with different oxidation states, which could be stabilized by the pulsed electrolysis method during CO<sub>2</sub>RR. On the basis of this method, we have studied the effect of the oxidation state of Cu on CO<sub>2</sub>RR to form C<sub>2+</sub> products. It has been found that the Cu catalyst with an oxidation state of +0.41 is the most efficient in our reaction system, and the FE of C<sub>2+</sub> products is 70.3% in an H-type cell. This work provides a precise method to identify the optimal oxidation state of the catalysts that are not stable in the reaction.

The electrocatalytic CO<sub>2</sub> reduction reaction (CO<sub>2</sub>RR) to form value-added carbon-based chemicals and fuels by utilizing renewable electricity is a promising technology to mitigate CO<sub>2</sub> emissions, fulfil the anthropogenic carbon cycle, and store excess renewable electricity as chemical energy.<sup>1–7</sup> Among the products that can be generated from CO<sub>2</sub>RR, C<sub>2+</sub> products are the most desirable due to their high energy densities and industrial value as chemical feedstocks.<sup>8–12</sup> However, their selectivity and activity are severely limited by multistep hydro-

genation and the sluggish kinetics of C–C coupling steps. To date, copper is known to be the most efficient electrocatalyst for selectively converting CO<sub>2</sub> to C<sub>2+</sub> products.<sup>13–16</sup> The synergism of Cu<sup>1+</sup> and Cu<sup>0</sup> sites in copper catalysts has been verified to achieve high faradaic efficiency (FE) for CO<sub>2</sub>-to-C<sub>2+</sub> products.<sup>17–20</sup> However, previous research has shown that Cu<sup>1+</sup> species are reduced to Cu<sup>0</sup> in the reaction.<sup>21–23</sup> Therefore, it is challenging to confirm the optimal Cu oxidation state for efficient electrocatalytic CO<sub>2</sub>RR.

Various strategies have been used to tune the Cu electron structure, such as space confinement,<sup>24,25</sup> the synthesis of alloys,<sup>26</sup> doping heteroatoms,<sup>27,28</sup> and organic ligand modification.<sup>29,30</sup> Among these, organic ligand modification (e.g. carboxylate and imidazole) has been reported to stabilize metal centers with appropriate oxidation states, and thus affects the intermediate adsorption during CO<sub>2</sub>RR.<sup>30–36</sup> Meanwhile, the Cu-based catalyst prepared by modifying the carboxylate ligand showed unique electrochemical CO<sub>2</sub> reduction selectivity toward C<sub>2+</sub> products.<sup>37–39</sup> This has made the method to be viewed as a good candidate for constructing Cu<sup>1+</sup> catalytic sites to promote the formation of C<sub>2+</sub> products. However, the content of Cu<sup>1+</sup> drops dramatically during the potentiostatic electrolysis, resulting in the change of CO<sub>2</sub>RR catalytic activity.

Pulsed potential electrolysis has emerged as a simple and effective method to increase the reaction durability and improve the product selectivity in CO<sub>2</sub>RR *via* tuning the surface architecture, oxidation state, surface adsorbate coverage and local pH.<sup>40–44</sup> Meanwhile, the pulsed electrochemical method is also a simple and quick method to prepare various materials, such as metals, alloys, metal chalcogenides and porous materials.<sup>45–49</sup> Recently, based on the pulsed electrolysis method, our group proposed the “*in situ* periodic regeneration of catalyst (PR-C)” strategy to give long-term high efficiency of CO<sub>2</sub> electroreduction to generate C<sub>2+</sub> products over the Cu catalyst by applying a positive potential pulse for a short time periodically in the halide-containing electrolyte.<sup>50</sup> At the same time, we also found that the Cu catalyst could be

<sup>a</sup>Beijing National Laboratory for Molecular Sciences, CAS Key Laboratory of Colloid and Interface and Thermodynamics, CAS Research/Education Center for Excellence in Molecular Sciences, Institute of Chemistry, Chinese Academy of Sciences, Beijing 100190, China. E-mail: sunxiaofu@iccas.ac.cn, hanbx@iccas.ac.cn

<sup>b</sup>School of Chemical Sciences, University of Chinese Academy of Sciences, Beijing 100049, China

<sup>c</sup>College of Chemical and Pharmaceutical Engineering, Hebei University of Science and Technology, Shijiazhuang 050018, China

<sup>d</sup>Shanghai Key Laboratory of Green Chemistry and Chemical Processes, School of Chemistry and Molecular Engineering, East China Normal University, Shanghai 200062, China

† Electronic supplementary information (ESI) available. See DOI: <https://doi.org/10.1039/d2gc04368h>

*in situ* regenerated to maintain the stability of the oxidation state of Cu *via* the pulsed potential electrocatalytic CO<sub>2</sub>RR.

Identifying the optimal oxidation state of Cu in CO<sub>2</sub>RR to form C<sub>2+</sub> products is of importance from both fundamental and practical points of views. Herein, we designed and prepared several Cu<sub>x</sub>C<sub>y</sub>O<sub>z</sub> catalysts with different Cu oxidation states using the pulsed electrochemical method. The oxidation state of Cu was stabilized by the pulsed potential in CO<sub>2</sub>RR, and the optimal oxidation state of Cu for producing C<sub>2+</sub> products was figured out. It was found that the catalyst with an average Cu valence state of 0.41 was most efficient, and the FE of C<sub>2+</sub> products could reach 70.3% with a current density of 24.1 mA cm<sup>-2</sup> at -1.0 V *versus* the reversible hydrogen electrode (RHE).

As illustrated in Fig. 1A, the catalysts were prepared *via* a pulsed electrochemical method in 0.1 M KHCO<sub>3</sub> aqueous electrolyte containing 0.1 M potassium benzenedicarboxylate (K<sub>2</sub>BDC). A typical H-type cell with three-electrode configuration was used in this work, which included a Cu foil working electrode, a Pt gauze counter electrode, and an Ag/AgCl reference electrode. Cu<sup>2+</sup> ions were generated at the anode potential ( $E_a = 1.25$  V *vs.* RHE), and they interacted with negatively charged carboxylate ligands to form the Cu complex. The Cu complex was then reduced to Cu<sub>x</sub>C<sub>y</sub>O<sub>z</sub> at the cathode potential

( $E_c = -1.0$  V *vs.* RHE). Anodic pulses ( $t_a$ ) of 3 s followed by cathodic pulses ( $t_c$ ) of 5 s were applied in this work. Such pulses were repeated for 80 cycles.

The scanning electron microscopy (SEM) image showed that the untreated Cu foil had a smooth surface (Fig. 1B). The Cu complex has a leaf-like structure generated by the stacking of lamellae due to the application of  $E_a$  (Fig. 1C). The X-ray diffraction (XRD) patterns in Fig. 1D confirmed the presence of a crystalline quasi-metal-organic framework (MOF).<sup>39</sup> After that, the electrochemical reconstruction<sup>51–53</sup> was performed by reducing the Cu complex in an electrolyte to form the Cu<sub>x</sub>C<sub>y</sub>O<sub>z</sub> catalyst. The leaf-like structure was converted into uniform nanoparticles (Fig. 1E). The high-resolution transmission electron microscopy (HR-TEM) image (Fig. 1F) confirmed that both metallic Cu and Cu<sub>2</sub>O crystal lattices existed in the Cu<sub>x</sub>C<sub>y</sub>O<sub>z</sub> catalyst, where 0.21 nm and 0.24 nm belong to Cu (111) and Cu<sub>2</sub>O(111), respectively.<sup>54,55</sup> This can also be confirmed from the XRD patterns (Fig. 1D). The corresponding energy-dispersive X-ray spectroscopy (EDS) results showed that the atomic ratio of Cu:C:O was approximately 4:2:1 (Table S1†). The EDS for elemental mapping (Fig. 1G) showed that the Cu, C and O elements were distributed homogeneously throughout the entire architectures.

The surface analysis of different samples was performed by quasi *in situ* X-ray photoelectron spectroscopy (XPS) (Fig. S1† and Fig. 1H). The Cu 2p XPS spectra and Cu Auger L<sub>3</sub>M<sub>45</sub>M<sub>45</sub> transition indicated that Cu<sup>2+</sup> was the major species in the Cu complex, while Cu<sup>0</sup> and Cu<sup>1+</sup> species existed in Cu<sub>x</sub>C<sub>y</sub>O<sub>z</sub>. Furthermore, the detailed structural information of Cu was investigated by *in situ* X-ray absorption spectroscopy (XAS) and X-ray emission spectroscopy (XES). As shown in Fig. 1I, Cu K-edge X-ray absorption near-edge spectroscopy (XANES) of the Cu complex exhibited an edge profile similar to that of CuO or Cu(OH)<sub>2</sub> in the range from 8960 to 9020 eV, while the spectrum of Cu<sub>x</sub>C<sub>y</sub>O<sub>z</sub> showed a close absorption edge with the Cu foil. These observations indicated that Cu in Cu<sub>x</sub>C<sub>y</sub>O<sub>z</sub> has a lower oxidation state compared with that in the Cu complex. Both the Cu complex and Cu<sub>x</sub>C<sub>y</sub>O<sub>z</sub> presented a characteristic Cu–Cu peak at 2.3 Å and a Cu–O peak at around 1.5 Å in the extended X-ray absorption fine-structure (EXAFS) spectra (Fig. S2†). However, the intensity of the Cu–O peak decreased and the intensity of the Cu–Cu peak increased in Cu<sub>x</sub>C<sub>y</sub>O<sub>z</sub> compared to those of the Cu complex, suggesting that the oxidized copper in the Cu complex was partially reduced during the formation of Cu<sub>x</sub>C<sub>y</sub>O<sub>z</sub>. Fig. 1J shows the Cu Kβ<sub>1,3</sub> XES spectra of the Cu complex and Cu<sub>x</sub>C<sub>y</sub>O<sub>z</sub>. When comparing the spectra with those of the reference samples, the *in situ* spectra for the Cu complex lay in between those for the Cu<sup>2+</sup> and Cu<sup>+</sup> references, whereas in the case of Cu<sub>x</sub>C<sub>y</sub>O<sub>z</sub>, the spectra were in between those for Cu<sup>1+</sup> and Cu<sup>0</sup>. Both the XAS and XES results indicated the co-existence of Cu<sup>1+</sup> and Cu<sup>0</sup> species in Cu<sub>x</sub>C<sub>y</sub>O<sub>z</sub>, which is in line with the XPS data.

It is worth noting that application of different  $E_a$  values would affect the oxidation state of Cu in the Cu<sub>x</sub>C<sub>y</sub>O<sub>z</sub> catalyst. As shown in Fig. 2A, we prepared a series of catalysts by changing the  $E_a$ . The SEM images are shown in Fig. S3,† and their

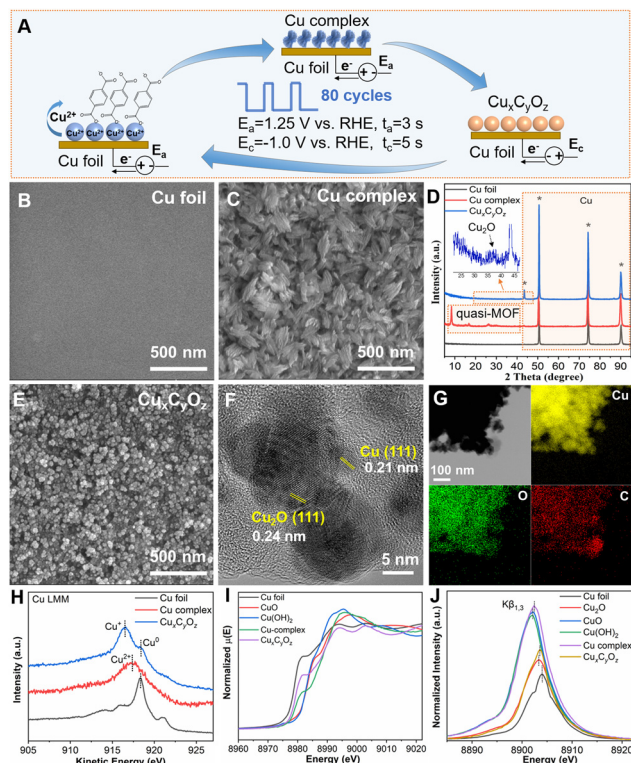


**Fig. 1** (A) Schematic diagram of the preparation of the Cu<sub>x</sub>C<sub>y</sub>O<sub>z</sub> catalyst. SEM images of (B) Cu foil, (C) Cu complex, and (E) Cu<sub>x</sub>C<sub>y</sub>O<sub>z</sub>. (D) XRD patterns of different samples. (F) HR-TEM image and (G) elemental mappings images of Cu<sub>x</sub>C<sub>y</sub>O<sub>z</sub>. (H) The quasi *in situ* XPS signals of Cu Auger LMM spectra for the Cu foil, Cu complex, and Cu<sub>x</sub>C<sub>y</sub>O<sub>z</sub>. (I) XANES spectra and (J) XES spectra of different samples.



**Fig. 2** (A) Schematic diagram of the preparation of the  $\text{Cu}_x\text{C}_y\text{O}_z$  catalyst under different conditions ( $E_a = 1.0$  V, 1.25 V, 1.4 V, and 1.6 V vs. RHE,  $t_a = 3$  s,  $E_c = -1.0$  V vs. RHE,  $t_c = 5$  s). (B) XANES spectra at the Cu K-edge under different conditions. (C) Average oxidation state of Cu in  $\text{Cu}_x\text{C}_y\text{O}_z$  under different conditions from Cu K-edge XANES.

morphologies were quite similar. The impact of the applied  $E_a$  on the Cu oxidation state was further investigated using XANES (Fig. 2B). The absorption edges of all the samples reside between those of  $\text{Cu}^0$  and  $\text{Cu}^{1+}$ . We also acquired the oxidation state of Cu as a function of the Cu K-edge energy shift (Fig. 2C). The detailed calculation method for quantifying the oxidation average valence state of Cu is discussed in the ESI (Table S2†). The average valence of Cu increased gradually with the increase of the applied  $E_a$ , which was +0.20, +0.41, +0.47 and +0.59, when the applied  $E_a$  was 1.0 V, 1.25 V, 1.4 V, and 1.6 V vs. RHE, respectively. For making a clear distinction, these  $\text{Cu}_x\text{C}_y\text{O}_z$  catalysts with different Cu oxidation states are denoted as  $\text{Cu}_x\text{C}_y\text{O}_z(0.20)$ ,  $\text{Cu}_x\text{C}_y\text{O}_z(0.41)$ ,  $\text{Cu}_x\text{C}_y\text{O}_z(0.47)$ , and  $\text{Cu}_x\text{C}_y\text{O}_z(0.59)$ .

Next, quasi *in situ* XPS and Auger LMM transition measurements were performed to characterize the composition and structure changes of the catalysts during the  $\text{CO}_2\text{RR}$  in different routes. In route (1), pulsed electrolysis ( $E_a = 1.25$  V vs. RHE,  $t_a = 3$  s;  $E_c = -1.0$  V vs. RHE,  $t_c = 50$  s) was applied in 0.1 M  $\text{KHCO}_3\text{-K}_2\text{BDC}$  electrolyte. The same electrolysis conditions as applied for the preparation of  $\text{Cu}_x\text{C}_y\text{O}_z$  catalyst were followed for the  $\text{CO}_2\text{RR}$ , except that the time of  $t_c$  was extended. In route (2), potentiostatic electrolysis was applied in 0.1 M  $\text{KHCO}_3\text{-K}_2\text{BDC}$  electrolyte with  $E_c = -1.0$  V vs. RHE. As shown in Fig. 3A and B, the content of  $\text{Cu}^{1+}$  could be maintained unchanged in route (1), while it would be decreased gradually in route (2). To further investigate the changes in the Cu oxidation state, operando XAS at the Cu K-edge was carried out. The Cu K-edge XANES spectra of  $\text{Cu}_x\text{C}_y\text{O}_z(0.41)$  used in route (1) for different times exhibited an edge profile similar to that of the catalyst before the reaction, while close to the absorption edge of the Cu foil when reacted in route (2) (Fig. 3C and D). On the other hand, the intensity of Cu–Cu coordination (2.3 Å) of  $\text{Cu}_x\text{C}_y\text{O}_z(0.41)$  in route (1) was basically unchanged compared to that of the catalyst before the reaction, but it gradually increased in route (2) in the Fourier transform (FT)



**Fig. 3** The quasi *in situ* Auger LMM spectra of Cu for  $\text{Cu}_x\text{C}_y\text{O}_z(0.41)$  reacted in (A) route (1) and (B) route (2) for different times. The *in situ* XANES spectra of  $\text{Cu}_x\text{C}_y\text{O}_z(0.41)$  reacted in (C) route (1) and (D) route (2) for different times.

of the EXAFS spectra in  $R$  space (Fig. S4†). The results demonstrated that the Cu oxidation state can be maintained by the *in situ* regeneration of  $\text{Cu}^{1+}$  during the  $\text{CO}_2\text{RR}$  in route (1), while it declined gradually to tend to  $\text{Cu}^0$  during the  $\text{CO}_2\text{RR}$  in route (2).

The  $\text{CO}_2\text{RR}$  performances of  $\text{Cu}_x\text{C}_y\text{O}_z$  catalysts were then investigated in an H-type cell under different electrolysis conditions for 2 h. We considered the effect of  $\text{K}^+$  concentration on the  $\text{CO}_2\text{RR}$  performance, and found that the increase of the  $\text{K}^+$  concentration in the electrolyte did not promote the formation of  $\text{C}_{2+}$  products (Fig. S5†). We also carried out the electrolysis experiments under a  $\text{N}_2$  atmosphere (without  $\text{CO}_2$ ). No carbon-based reduction product could be detected, indicating that  $\text{CO}_2$  was the carbon source in this work. For  $\text{Cu}_x\text{C}_y\text{O}_z(0.41)$ , it had a higher current density at  $-0.9$  to  $-1.25$  V vs. RHE in route (1) than that in route (2) (Fig. 4A and B). Route (1) also showed a significant difference in the distributions of  $\text{CO}_2\text{RR}$  products compared with route (2).  $\text{C}_1$  products (CO, formate and methane),  $\text{C}_{2+}$  products (ethylene, ethanol and *n*-propanol) and  $\text{H}_2$  can be detected by  $^1\text{H}$  nuclear magnetic resonance (NMR) spectroscopy and gas chromatography (GC). The FE for  $\text{C}_{2+}$  products in route (1) was much higher than that in route (2). In route (1), the  $\text{Cu}_x\text{C}_y\text{O}_z(0.41)$  catalyst exhibits a volcano-shaped dependence of total FE for  $\text{C}_{2+}$  products at different  $E_c$  values, and the maximum FE ( $\text{C}_{2+}$  products) could reach up to 70.3% at  $-1.0$  V vs. RHE with a current density of  $24.1 \text{ mA cm}^{-2}$ , while the highest FE for  $\text{C}_{2+}$  products was only 46.6% in route (2). The catalyst also showed



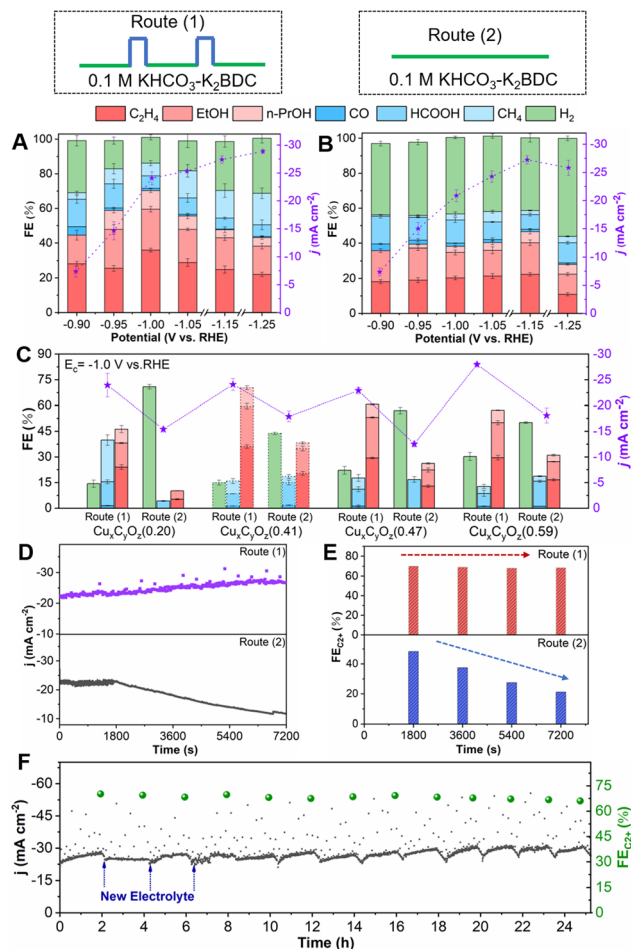


**Fig. 4** CO<sub>2</sub>RR product distribution and current density ( $j$ ) of Cu<sub>*x*</sub>C<sub>*y*</sub>O<sub>*z*</sub>(0.41) in (A) route (1) and (B) route (2). (C) CO<sub>2</sub>RR product distribution and current density of Cu<sub>*x*</sub>C<sub>*y*</sub>O<sub>*z*</sub> with different oxidation states of Cu. (D and E) Dependence of the current density ( $j$ ) and FE of Cu<sub>*x*</sub>C<sub>*y*</sub>O<sub>*z*</sub>(0.41) on time in route (1) and route (2). (F) Long-term stability of CO<sub>2</sub> pulsed electroreduction over Cu<sub>*x*</sub>C<sub>*y*</sub>O<sub>*z*</sub>(0.41).

lower CO<sub>2</sub>RR performance to form C<sub>2+</sub> products in routes (3) and (4) in 0.1 M KHCO<sub>3</sub> (Fig. S6†).

Furthermore, the CO<sub>2</sub>RR performance of other Cu<sub>*x*</sub>C<sub>*y*</sub>O<sub>*z*</sub> catalysts was also evaluated. The Cu<sub>*x*</sub>C<sub>*y*</sub>O<sub>*z*</sub>(0.41) catalyst exhibited an optimal CO<sub>2</sub>-to-C<sub>2+</sub> product performance with the average Cu valence state of 0.41 under an  $E_a$  of 1.25 V (Fig. 4C). In the control experiments, we optimized the duration of the pulse ( $t_a$  and  $t_c$ ) and the concentration of the electrolyte. The detailed discussion is shown in the ESI (Fig. S7–S12†). The final optimized reaction conditions are  $E_a = 1.25$  V vs. RHE,  $t_a = 3$  s,  $E_c = -1.0$  V vs. RHE,  $t_c = 50$  s, and the FE of C<sub>2+</sub> products was the highest in the electrolyte containing 0.1 M K<sub>2</sub>BDC.

Based on the above analysis, some important observations are summarized below.

(1) The pulsed electrolysis can effectively inhibit the hydrogen evolution reaction (HER) and promote the formation of C<sub>2+</sub> products.

(2) The addition of K<sub>2</sub>BDC in the electrolyte did not contribute to the formation of C<sub>2+</sub> products by comparing to that in routes (2) and (4) under potentiostatic electrolysis conditions (Fig. 4B and Fig. S6B†), while the addition of K<sub>2</sub>BDC in the electrolyte combined with pulsed electrolysis can achieve the *in situ* regeneration of the Cu<sub>*x*</sub>C<sub>*y*</sub>O<sub>*z*</sub> catalyst to stabilize the oxidation state of Cu during the pulsed CO<sub>2</sub>RR, leading to the improved CO<sub>2</sub>-to-C<sub>2+</sub> performance.

(3) The oxidation state of Cu in Cu<sub>*x*</sub>C<sub>*y*</sub>O<sub>*z*</sub> catalysts could regulate the CO<sub>2</sub>-to-C<sub>2+</sub> product performance. The optimal oxidation state of Cu in Cu<sub>*x*</sub>C<sub>*y*</sub>O<sub>*z*</sub> catalysts was +0.41 corresponding to the best CO<sub>2</sub>-to-C<sub>2+</sub> performance.

(4) The SEM images show that there was no obvious change after different reaction times in route (1) and route (2) (Fig. S13†), suggesting that the K<sub>2</sub>BDC in the electrolyte did not change the morphology of the catalyst, which also confirmed that the change in CO<sub>2</sub>RR performance did not originate from the variation of the catalyst morphology.

The stability was crucial for the application of CO<sub>2</sub>RR. First, the current density of CO<sub>2</sub>RR and the FE of C<sub>2+</sub> products, which depend on the reaction time within 2 h, were investigated. Obviously, the current density and FE of C<sub>2+</sub> products over the Cu<sub>*x*</sub>C<sub>*y*</sub>O<sub>*z*</sub>(0.41) catalyst did not change significantly with time in route (1), while both of them decreased continuously in route (2) (Fig. 4D and E). The Cu<sub>*x*</sub>C<sub>*y*</sub>O<sub>*z*</sub> catalysts with the other oxidation states of Cu also show a similar phenomenon (Fig. S14†). Furthermore, consecutive cycles were carried out to determine the long-term CO<sub>2</sub>RR stability of the Cu<sub>*x*</sub>C<sub>*y*</sub>O<sub>*z*</sub>(0.41) catalyst in route (1). The current density and FE of C<sub>2+</sub> products did not change notably over 25 hours in route (1) (Fig. 4F). The results demonstrated that Cu<sub>*x*</sub>C<sub>*y*</sub>O<sub>*z*</sub>(0.41) exhibited outstanding catalytic activity and stability toward CO<sub>2</sub>RR in route (1) due to the fact that Cu in the catalyst has an optimal oxidation state and can be maintained by the *in situ* regeneration of Cu during the reaction.

## Conclusions

In summary, the Cu<sub>*x*</sub>C<sub>*y*</sub>O<sub>*z*</sub> catalysts with different Cu oxidation states have been synthesized *via* the pulsed electrochemical method. The oxidation state of Cu can be stabilized by the pulsed anode potential in CO<sub>2</sub>RR, which allows us to study the effect of the oxidation state of Cu on the performance of the catalysts more precisely. It is found that the FEs of C<sub>2+</sub> products depend strongly on the oxidation state of Cu. The catalyst with a Cu oxidation state of +0.41 yields the highest C<sub>2+</sub> FE of 70.3% with a current density of 24.1 mA cm<sup>-2</sup> in an H-type cell. This work provides a precise method to identify the optimal oxidation state of the catalysts. This method is specifically favorable for studying the catalysts that are not stable during the electrochemical reaction due to the reduction of the active species. Obviously, it is also useful for designing efficient catalysts with a suitable oxidation state for CO<sub>2</sub>RR.

## Author contributions

L. X., X. F. S. and B. X. H. proposed the project, designed the experiments, and wrote the manuscript. L. X. performed the whole experiments. J. Q. F., L. M. W., X. N. S. and X. X. T. performed the analysis of experimental data. L. B. Z., X. D. M. and S. H. J. conducted a part of the characterization study. J. D. and A. B. C. participated in discussions. X. F. S. and B. X. H. supervised the whole project.

## Conflicts of interest

There are no conflicts to declare.

## Acknowledgements

The work was supported by the National Natural Science Foundation of China (22002172, 22203099 and 22121002), the Beijing Natural Science Foundation (J210020), the S&T Program of Hebei (B2021208074), the Chinese Academy of Sciences (QYZDY-SSW-SLH013) and the Photon Science Center for Carbon Neutrality. The X-ray absorption spectroscopy measurements were performed at Beamline 4B9A at Beijing Synchrotron Radiation Facility (BSRF). The X-ray emission spectroscopy beam time was granted by Beamline 4W1B of BSRF, Institute of High Energy Physics, Chinese Academy of Sciences. The staff members of 4W1B are acknowledged for their support in measurements and data reduction.

## References

- W. Ma, X. He, W. Wang, S. Xie, Q. Zhang and Y. Wang, *Chem. Soc. Rev.*, 2021, **50**, 12897–12914.
- R. B. Song, W. Zhu, J. Fu, Y. Chen, L. Liu, J. R. Zhang, Y. Lin and J. J. Zhu, *Adv. Mater.*, 2020, **32**, 1903796.
- D. Gao, P. Wei, H. Li, L. Lin, G. Wang and X. Bao, *Acta Phys.-Chim. Sin.*, 2021, **37**, 2009021.
- X. Song, L. Xu, X. Sun and B. Han, *Sci. China: Chem.*, 2023, **66**, 315–323.
- W. Guo, S. Liu, X. Tan, R. Wu, X. Yan, C. Chen, Q. Zhu, L. Zheng, J. Ma, J. Zhang, Y. Huang, X. Sun and B. Han, *Angew. Chem., Int. Ed.*, 2021, **60**, 21979–21987.
- J. H. Ye, T. Ju, H. Huang, L. L. Liao and D. G. Yu, *Acc. Chem. Res.*, 2021, **54**, 2518–2531.
- D. G. Yu and L. N. He, *Green Chem.*, 2021, **23**, 3499–3501.
- H. L. Zhu, H. Y. Chen, Y. X. Han, Z. H. Zhao, P. Q. Liao and X. M. Chen, *J. Am. Chem. Soc.*, 2022, **144**, 13319–13326.
- W. Liu, P. Zhai, A. Li, B. Wei, K. Si, Y. Wei, X. Wang, G. Zhu, Q. Chen, X. Gu, R. Zhang, W. Zhou and Y. Gong, *Nat. Commun.*, 2022, **13**, 1877.
- J. E. Huang, F. Li, A. Ozden, A. S. Rasouli, F. P. García de Arquer, S. Liu, S. Zhang, M. Luo, X. Wang, Y. Lum, Y. Xu, K. Bertens, R. K. Miao, C. T. Dinh, D. Sinton and E. H. Sargent, *Science*, 2021, **372**, 1074–1078.
- Y. Zhao, X. Zu, R. Chen, X. Li, Y. Jiang, Z. Wang, S. Wang, Y. Wu, Y. Sun and Y. Xie, *J. Am. Chem. Soc.*, 2022, **144**, 10446–10454.
- X. Yan, C. Chen, Y. Wu, Y. Chen, J. Zhang, R. Feng, J. Zhang and B. Han, *Green Chem.*, 2022, **24**, 1989–1994.
- Y. Wang, J. Liu and G. Zheng, *Adv. Mater.*, 2021, **33**, 2005798.
- C. Xiao and J. Zhang, *ACS Nano*, 2021, **15**, 7975–8000.
- Y. Zhang, P. Li, C. Zhao, G. Zhou, F. Zhou, Q. Zhang, C. Su and Y. Wu, *Sci. Bull.*, 2022, **67**, 1679–1687.
- C. Liu, J. Gong, Z. Gao, L. Xiao, G. Wang, J. Lu and L. Zhuang, *Sci. China: Chem.*, 2021, **64**, 1660–1678.
- L. Ding, N. Zhu, Y. Hu, Z. Chen, P. Song, T. Sheng, Z. Wu and Y. Xiong, *Angew. Chem., Int. Ed.*, 2022, **61**, e202209268.
- T. C. Chou, C. C. Chang, H. L. Yu, W. Y. Yu, C. L. Dong, J. J. Velasco-Vélez, C. H. Chuang, L. C. Chen, J. F. Lee, J. M. Chen and H. L. Wu, *J. Am. Chem. Soc.*, 2020, **142**, 2857–2867.
- Y. Zhou, Y. Yao, R. Zhao, X. Wang, Z. Fu, D. Wang, H. Wang, L. Zhao, W. Ni, Z. Yang and Y. M. Yan, *Angew. Chem., Int. Ed.*, 2022, **61**, e202205832.
- J. Wang, H. Y. Tan, Y. Zhu, H. Chu and H. M. Chen, *Angew. Chem., Int. Ed.*, 2021, **60**, 17254–17267.
- Z. Z. Wu, F. Y. Gao and M. R. Gao, *Energy Environ. Sci.*, 2021, **14**, 1121–1139.
- S. Popovic, M. Smiljanic, P. Jovanovic, J. Vavra, R. Buonsanti and N. Hodnik, *Angew. Chem., Int. Ed.*, 2020, **59**, 14736–14746.
- X. Yuan, S. Chen, D. Cheng, L. Li, W. Zhu, D. Zhong, Z. Zhao, J. Li, T. Wang and J. Gong, *Angew. Chem., Int. Ed.*, 2021, **60**, 15344–15347.
- P. P. Yang, X. L. Zhang, F. Y. Gao, Y. R. Zheng, Z. Z. Niu, X. Yu, R. Liu, Z. Z. Wu, S. Qin, L. P. Chi, Y. Duan, T. Ma, X. S. Zheng, J. F. Zhu, H. J. Wang, M. R. Gao and S. H. Yu, *J. Am. Chem. Soc.*, 2020, **142**, 6400–6408.
- J. Y. Kim, D. Hong, J. C. Lee, H. G. Kim, S. Lee, S. Shin, B. Kim, H. Lee, M. Kim, J. Oh, G. D. Lee, D. H. Nam and Y. C. Joo, *Nat. Commun.*, 2021, **12**, 3765.
- F. Hu, L. Yang, Y. Jiang, C. Duan, X. Wang, L. Zeng, X. Lv, D. Duan, Q. Liu, T. Kong, J. Jiang, R. Long and Y. Xiong, *Angew. Chem., Int. Ed.*, 2021, **60**, 26122–26127.
- W. He, I. Liberman, I. Rozenberg, R. Ifraemov and I. Hod, *Angew. Chem., Int. Ed.*, 2020, **59**, 8262–8269.
- Z. Yin, C. Yu, Z. Zhao, X. Guo, M. Shen, N. Li, M. Muzzio, J. Li, H. Liu, H. Lin, J. Yin, G. Lu, D. Su and S. Sun, *Nano Lett.*, 2019, **19**, 8658–8663.
- H. L. Zhu, J. R. Huang, X. W. Zhang, C. Wang, N. Y. Huang, P. Q. Liao and X. M. Chen, *ACS Catal.*, 2021, **11**, 11786–11792.
- Q. Fan, X. Zhang, X. Ge, L. Bai, D. He, Y. Qu, C. Kong, J. Bi, D. Ding, Y. Cao, X. Duan, J. Wang, J. Yang and Y. Wu, *Adv. Energy Mater.*, 2021, **11**, 2101424.
- Q. Zhu, C. J. Murphy and L. R. Baker, *J. Am. Chem. Soc.*, 2022, **144**, 2829–2840.
- X. F. Qiu, H. L. Zhu, J. R. Huang, P. Q. Liao and X. M. Chen, *J. Am. Chem. Soc.*, 2021, **143**, 7242–7246.

- 33 L. Zhang, X. X. Li, Z. L. Lang, Y. Liu, J. Liu, L. Yuan, W. Y. Lu, Y. S. Xia, L. Z. Dong, D. Q. Yuan and Y. Q. Lan, *J. Am. Chem. Soc.*, 2021, **143**, 3808–3816.
- 34 L. Hao, Q. Xia, Q. Zhang, J. Masa and Z. Sun, *Chin. J. Catal.*, 2021, **42**, 1903–1920.
- 35 Y. Yang, Z. Zhang, Z. Zhang, C. Tang, X. Chang and L. Duan, *Chin. J. Chem.*, 2021, **39**, 1281–1287.
- 36 Y. Wang, X. P. Zhang, H. Lei, K. Guo, G. Xu, L. Xie, X. Li, W. Zhang, U. P. Apfel and R. Cao, *CCS Chem.*, 2022, **4**, 2959–2967.
- 37 K. Yao, Y. Xia, J. Li, N. Wang, J. Han, C. Gao, M. Han, G. Shen, Y. Liu, A. Seifitokaldani, X. Sun and H. Liang, *J. Mater. Chem. A*, 2020, **8**, 11117–11123.
- 38 Q. Zhu, X. Sun, D. Yang, J. Ma, X. Kang, L. Zheng, J. Zhang, Z. Wu and B. Han, *Nat. Commun.*, 2019, **10**, 3851.
- 39 W. Zhang, C. Huang, J. Zhu, Q. Zhou, R. Yu, Y. Wang, P. An, J. Zhang, M. Qiu, L. Zhou, L. Mai, Z. Yi and Y. Yu, *Angew. Chem., Int. Ed.*, 2022, **61**, e202112116.
- 40 R. Casebolt, K. Levine, J. Suntivich and T. Hanrath, *Joule*, 2021, **5**, 1987–2026.
- 41 C. Kim, J. C. Bui, X. Luo, J. K. Cooper, A. Kusoglu, A. Z. Weber and A. T. Bell, *Nat. Energy*, 2021, **6**, 1026–1034.
- 42 R. M. Arán-Ais, F. Scholten, S. Kunze, R. Rizo and B. R. Cuenya, *Nat. Energy*, 2020, **5**, 317–325.
- 43 H. S. Jeon, J. Timoshenko, C. Rettenmaier, A. Herzog, A. Yoon, S. W. Chee, S. Oener, U. Hejral, F. T. Haase and B. Roldan Cuenya, *J. Am. Chem. Soc.*, 2021, **143**, 7578–7587.
- 44 J. Timoshenko, A. Bergmann, C. Rettenmaier, A. Herzog, R. M. Arán-Ais, H. S. Jeon, F. T. Haase, U. Hejral, P. Grosse, S. Kühn, E. M. Davis, J. Tian, O. Magnussen and B. R. Cuenya, *Nat. Catal.*, 2022, **5**, 259–267.
- 45 J. Li, Y. Kuang, Y. Meng, X. Tian, W. H. Hung, X. Zhang, A. Li, M. Xu, W. Zhou, C. S. Ku, C. Y. Chiang, G. Zhu, J. Guo, X. Sun and H. Dai, *J. Am. Chem. Soc.*, 2020, **142**, 7276–7282.
- 46 K. Jiang, R. B. Sandberg, A. J. Akey, X. Liu, D. C. Bell, J. K. Nørskov, K. Chan and H. Wang, *Nat. Catal.*, 2018, **1**, 111–119.
- 47 Y. T. Huang, H. Lee, W. D. Li and S. P. Feng, *J. Power Sources*, 2019, **435**, 226801.
- 48 Y. Wang, Z. Meng, H. Chen, T. Li, D. Zheng, Q. Xu, H. Wang, X. Y. Liu and W. Guo, *J. Mater. Chem. C*, 2019, **7**, 1966–1973.
- 49 J. Chen, Y. Wang, J. Cao, L. Liao, Y. Liu, Y. Zhou, J. H. Ouyang, D. Jia, M. Wang, X. Li and Z. Li, *Electrochim. Acta*, 2020, **361**, 137036.
- 50 L. Xu, X. Ma, L. Wu, X. Tan, X. Song, Q. Zhu, C. Chen, Q. Qian, Z. Liu, X. Sun, S. Liu and B. Han, *Angew. Chem., Int. Ed.*, 2022, **61**, e202210375.
- 51 M. B. Kale, R. A. Borse, A. Gomaa Abdelkader Mohamed and Y. Wang, *Adv. Funct. Mater.*, 2021, **31**, 2101313.
- 52 T. Kim and G. T. R. Palmore, *Nat. Commun.*, 2020, **11**, 3622.
- 53 Z. Weng, Y. Wu, M. Wang, J. Jiang, K. Yang, S. Huo, X. F. Wang, Q. Ma, G. W. Brudvig, V. S. Batista, Y. Liang, Z. Feng and H. Wang, *Nat. Commun.*, 2018, **9**, 415.
- 54 Y. Zhong, X. Kong, Z. Song, Y. Liu, L. Peng, L. Zhang, X. Luo, J. Zeng and Z. Geng, *Nano Lett.*, 2022, **22**, 2554–2560.
- 55 Z. Chen, T. Wang, B. Liu, D. Cheng, C. Hu, G. Zhang, W. Zhu, H. Wang, Z. J. Zhao and J. Gong, *J. Am. Chem. Soc.*, 2020, **142**, 6878–6883.